

Exploring the Use of Orientation-Independent Inelastic Spectral Displacements in the Seismic Assessment of Bridges

Savvinos Aristeidou & G. J. O'Reilly

To cite this article: Savvinos Aristeidou & G. J. O'Reilly (22 Apr 2024): Exploring the Use of Orientation-Independent Inelastic Spectral Displacements in the Seismic Assessment of Bridges, *Journal of Earthquake Engineering*, DOI: [10.1080/13632469.2024.2343067](https://doi.org/10.1080/13632469.2024.2343067)

To link to this article: <https://doi.org/10.1080/13632469.2024.2343067>



Published online: 22 Apr 2024.



Submit your article to this journal



View related articles



View Crossmark data



Exploring the Use of Orientation-Independent Inelastic Spectral Displacements in the Seismic Assessment of Bridges

Savvino Aristeidou  and G. J. O'Reilly 

Centre for Training and Research on Reduction of Seismic Risk (ROSE Centre), Scuola Universitaria Superiore IUSS Pavia, Pavia, Italy

ABSTRACT

Seismic intensity measures (IMs) provide a link between the seismic hazard and the dynamic response of structures subjected to earthquake shaking. The spectral acceleration at the first and usually dominant vibration mode, $Sa(T_1)$, is a popular choice for building structures. Meanwhile, the IM selection for bridges is non-trivial since they do not typically possess a single dominant mode. Even for ordinary bridges with a dominant mode, the behavior can change significantly in each principal direction through the activation, or yielding, of its different components. This study examines the performance of a novel IM that incorporates ground motion directionality and structure non-linearity in this context: the nn^{th} percentile of all rotation angles of the inelastic spectral displacement, $Sd_{i,\text{RotDnn}}$. This evaluation is carried out within the context of an ordinary bridge structure and is compared with other conventional IMs used in regional risk assessment of bridges. The case study bridge utilized is a highway overcrossing located in California with two spans and a continuous prestressed reinforced concrete box girder deck section. A large ground motion set was selected from the NGA-West2 database, and incremental dynamic analysis was carried out on the structure to assess the IM performance to characterize collapse. The results indicate that $Sd_{i,\text{RotDnn}}$ performs very well compared to other IMs for the bridge structure and could be a prudent choice to characterize inelastic response of bridges with several possible mechanisms in different principal directions. Also, using the *RotD50* definition, typically used in ground motion models, showed a 17.3% increase in efficiency compared to *RotD100* definition typically used in engineering practice.

ARTICLE HISTORY

Received 22 June 2023
Accepted 9 April 2024

KEYWORDS

Bridge; PBEE; intensity measure; risk assessment; incremental dynamic analysis; directionality

1. Introduction

Bridges as part of road networks in seismically prone areas provide critical lifelines during substantial seismic events in addition to their fundamental role in the daily operation of society. Therefore, it is essential to maintain their serviceability under a wide range of earthquake intensities. While direct monetary losses can be significant, indirect losses may contribute substantially to the overall impact (Kilanitis and Sextos 2019) as there might be some degree of rerouting of the traffic demand, causing delays and therefore economic losses, if several bridges close for repairs. For instance, Enke et al. (2008) found for one scenario that indirect losses were about 55% of the direct losses, whereas another study by Abarca et al. (2022) discussed how because of the bridge's strategic importance the indirect impacts of the 2018 Polcevera bridge collapse in Italy were around ten times those of the direct costs, and another case study investigation in that same work by Abarca et al. (2022) in southern Italy showed the indirect losses to be approximately four times higher than the direct losses. Hence, assessment of bridge network resilience on a regional scale can be more insightful for community

impact. Nevertheless, many observations and contributions to these assessment methodologies are first developed on specific issues using smaller case studies.

To evaluate the seismic risk associated with a structure, fragility functions are used to express the probability of the structure being in different damage states. This information is then utilized in decision-making processes. One of the key components of fragility functions is the intensity measure (IM). It connects the level (or intensity) of ground shaking to the structure's damage state. Thus, it is an inseparable link within the performance-based earthquake engineering (PBEE) framework (Cornell and Krawinkler 2000), and should be chosen wisely depending on the type of structure and underlying seismic hazard conditions at hand.

Apart from the IM itself, its horizontal component definition is often overlooked but must also be considered, especially when the directionality effect of ground shaking is notable and is of interest to the particular structure typology being investigated. While the geometric mean has commonly been used to combine the two horizontal as-recorded orientations, more recent studies (Fayaz, Medalla, and Zareian 2020b; Y. Lin, He, and Igarashi 2022; Qian and Dong 2020) have opted for using the *RotDnn* component as proposed by Boore (2010). The *RotDnn* is defined as the nn^{th} fractile of a response spectral value for all rotation angles sorted by amplitude, where D stands for period-dependent rotation angle. The most commonly used definitions are the *RotD50* and *RotD100*, which are the spectral median value and the spectral maximum over all rotation angles, respectively. These definitions are not to be confused with the *RotDnn* horizontal component definition of the engineering demand parameter (EDP) obtained by rotating the ground motions to different incidence angles and imposing them to the structure (i.e. the output of dynamic structural analysis as opposed to the input). Herein, these horizontal component definitions were examined only for the IMs, not for the EDPs, in other words the directionality was considered as solely a property of ground motion and issues relating to angle of incidence were not explored.

For bridge structures, peak ground acceleration (PGA) and spectral acceleration-based, $Sa(T)$, IMs have traditionally been popular (Borzi et al. 2015). Still, it was suggested (Huang, Gardoni, and Hurlebaus 2010) that peak ground velocity (PGV) may also be useful. Inelastic spectral displacement has also been considered as an IM, first by Luco and Cornell (2007) and Tothong and Luco (2007), and more recently by Wu et al. (2019) for bridge structures, exploring its potential in probabilistic seismic demand analysis. The use of inelastic spectral displacement seeks to capture the displacement experienced by a simple oscillator proxy structure during an earthquake, which is a critical factor in determining the extent of damage in actual structures. Inelastic deformations are better associated with damage in the piers, such as permanent cracking, concrete spalling, fracture or buckling of reinforcing bars, or crushing of the core concrete due to fracture of the confining reinforcement (Tothong and Cornell 2006).

Hence, this paper explores a newly developed $Sd_{i,\text{RotD}50}$ IM that could be an improved means to accurately estimate inelastic deformation and collapse performance in bridge structures. Its horizontal component definition is the same with the one previously defined, but with inelastic spectral displacement as the spectral value. Also examined is the performance of different *RotDnn* (and generally horizontal component) definitions, for both elastic and inelastic spectral values, for a case study bridge structure. By performance, it is meant the comparative evaluation based on the relative efficiency and sufficiency of different IMs used for the seismic risk assessment of bridge structures. This research will contribute to a better understanding of appropriate IMs for bridge structures, where Sd_i ranks among them, and the relevance of the *RotDnn* component definitions in capturing the directionality of ground motion shaking. In Section 2, a brief literature review of works that studied the effects of directionality in the seismic assessment of bridges is given, along with some critical discussion. In Sections 3–5, the case study structure, ground motions considered, and intensity measures compared are reported, respectively. In Section 6, the different IMs and their horizontal component definitions are compared and ranked based on their sufficiency and efficiency. The extent at which the directionality of ground motions is biasing the seismic response of the bridge is explored specifically in Section 6.3. General discussion and conclusions are given in Section 7.

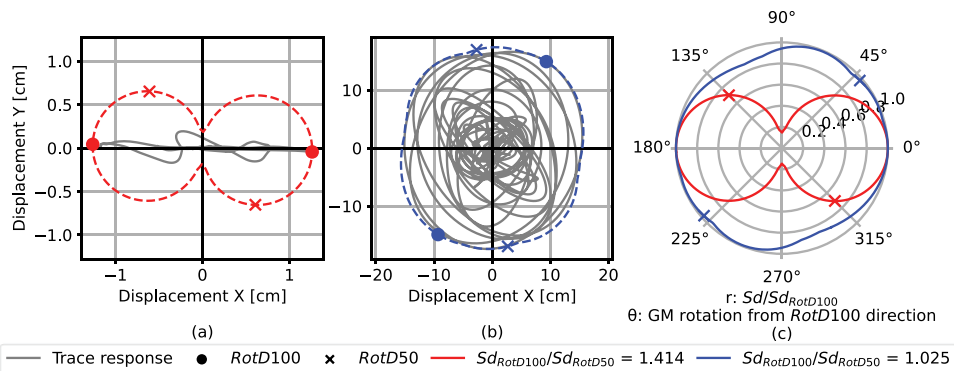


Figure 1. Trace response of an SDOF oscillator with $T = 2$ s. (a) Strongly directional ground motion (SMART1 007 recording from the 1985 Taiwan SMART1(33) earthquake, RSN: 492) and (b) non-directional ground motion (Dumbarton Bridge West End FF recording from the 1989 Loma Prieta earthquake, RSN: 757) and (c) the polar plot of normalized spectral displacement in all horizontal directions for the two records.

2. Directionality Effects in the Assessment of Bridges

Directionality effects, as illustrated in Fig. 1, are especially present in near-fault ground motions with forward directivity (Tarbali 2017) and fling-step characteristics, which are generally characterized by a unidirectional large-amplitude velocity pulse and a monotonic step in the displacement time history (Kalkan and Kunnath 2006). It is important to underline here that the characteristics of these motions, typically, have the biggest effect in the fault-normal direction and specifically the spectral acceleration at periods longer than 0.6 s (Somerville et al. 1997). Poulos and Miranda (2023) presented a modification for ground motion models (GMMs) to estimate the spectral acceleration at any given azimuth relative to the fault, which is useful when one knows the orientation of a strike-slip fault that governs the seismicity at a site, and also the main orientations of the structure being assessed or designed. However, this information may not always be available. Intensity measures that incorporate spectral values from all the possible rotation angles in the horizontal plane, e.g. *RotD*50, have the advantage of removing the sensor orientation as a contributor to epistemic uncertainty (Boore, Watson-Lamprey, and Abrahamson 2006) and they are state-of-the-art horizontal component definitions of spectral values. Additionally, when combined with the *RotD*100 definition in the appropriate manner (i.e. *RotD*100/*RotD*50) they can create a simple and useful measure of ground motion directionality, as depicted in Fig. 1. It should be noted that there are many proposed formulations of directionality measure in the literature (e.g. Rivera-Figueroa and Montejo 2022), however there is no common consensus of what scalar value can better describe the ground motion directionality. Nonetheless, the most prevalent in the literature seems to be the *RotD*100/*RotD*50 (Shahi and Baker 2014), so that was chosen for the comparisons herein. In this study, the elastic and inelastic spectral quantities computed from different horizontal component definitions were compared, in order to draw conclusions on which definition is more suitable as an IM choice for bridges.

Current seismic design methodologies (e.g. ASCE 7-16, Eurocode8, and JRA) do not specify the expected degree of directionality of a bi-directional ground motion shaking (Y. Lin, He, and Igarashi 2022). The latter imposes a complex combination of forces and displacements on the different components of a bridge structure (e.g. pier elements, shear keys, abutments). On that note, it has been noted in the literature that certain structural typologies, including highway bridges, are sensitive to input records with intense directionality effects (Mackie, Cronin, and Nielson 2011). That is because these structures often possess asymmetric stiffness, damping and strength characteristics. Several studies have noted and investigated this effect on bridges (Feng et al. 2018; Mackie, Cronin, and Nielson 2011; Sengupta et al. 2016; Torbol and Shinozuka 2014). Feng et al. (2018) assessed ten commonly used IMs, in terms of various metrics, to determine which ones better account for the

influence of incidence angle variation. This was also examined for various components of the bridge and the bridge system in general. It was found that the seismic excitation direction has a minor impact on the optimal IM rankings. Similar topics were addressed in a subsequent study (Feng, Yuan, and Sextos 2021), where the basis of comparison was the performance (i.e. monetary repair loss) of a horizontally curved bridge. Also, 20 candidate IMs were investigated and compared. An important finding was that the total bridge loss gradually becomes independent of the seismic excitation direction as the seismic intensity increases and the structure sustains heavier damage. It was also concluded that velocity-related and/or structure-dependent IMs presented superior performance, compared to other categories of IMs. Additionally, for different EDPs in different components, the critical incidence angle can vary significantly. Nevertheless, it was demonstrated in the literature (Mackie, Cronin, and Nielson 2011) that if the ground motion ensemble is of substantial size and representative of underlying hazard conditions at the site, the incidence angle does not have a significant effect on the response. The three aforementioned studies, though, included both polarized and unpolarized ground motions from both near- and far-field ranges, there was no distinction and direct comparison between polarized and unpolarized ground motions. Additionally, for the incidence angle to have a significant effect, all ground motions could be rotated so that the *RotD100* orientation (or fault-normal orientation for near-fault ground motions) coincides with the weaker principal structural direction. However, a significant bias would be introduced in such case since that would be the worst possible scenario regarding the incidence angle of each ground motion. Nevertheless, comparing that with the structural response obtained under randomly (or as-recorded) oriented ground motions would yield important insights on the most adverse effects that their directionality can have on a site.

3. Case Study Bridge Structure and Numerical Modelling

To illustrate the relative performance of these novel IMs for bridges, a case study structure was numerically modelled and analyzed for comparison. The structure adopted in this study was an existing bridge in California constructed in 2001. This bridge is the Jack Tone Road On-Ramp Overcrossing and has been used in several past studies (e.g. Fayaz, Dabaghi and Zareian 2020a; Otárola, Fayaz, and Galasso 2022). It is used here as a reference structure since much technical documentation is available for sufficiently detailed numerical modelling. It falls under the ordinary reinforced concrete bridge typology, with seat-type abutments, single-pier bent and box-girder deck.

A three-dimensional finite-element model was developed using the open-source software OpenSeesPy (Zhu, McKenna, and Scott 2018), whose parameters are described below. For the seismic analysis of bridge structures, it is typically not necessary to model a full three-dimensional model of the superstructure with detailed finite elements. Instead, simple spine models suffice for the scope of seismic analysis, provided that they represent the effective dynamic stiffness characteristics and mass distributions appropriately (Priestley, Seible, and Calvi 1996). Figure 2 depicts a schematic representation of the three-dimensional finite element model developed.

Since the bridge's superstructure is designed to remain elastic during earthquake-induced ground shaking, the deck was modelled with an *elasticBeamColumn* element in OpenSeesPy, with gross cross-sectional properties (i.e. $I_{\text{eff}} = I_g$), as recommended by Caltrans SDC (Caltrans 2019). The mass of the superstructure was modelled as a consistent distributed mass acting on the pier element and throughout the length of the deck elements, with each span discretized into ten elements. The bridge pier was modelled using the *forceBeamColumn* element, with fibre-based cross-sections, employing the *HingeRadau* integration method (Scott and Fenves 2006; Scott and Ryan 2013). The pier was assumed to be fixed at the base for simplicity and monolithically connected to the underside of the deck. Confined and unconfined concrete fibres were modelled using the *Concrete01* uniaxial material model, and the steel rebars were represented using the *Steel02* (i.e. Giuffre-Menegotto-Pinto) material model, including a *MinMax* limiting strain of $\varepsilon_{\text{su}} = 0.10$ (Priestley, Seible, and Calvi 1996) to capture the potential buckling and rupture of the steel reinforcing rebars. The plasticity in the piers was

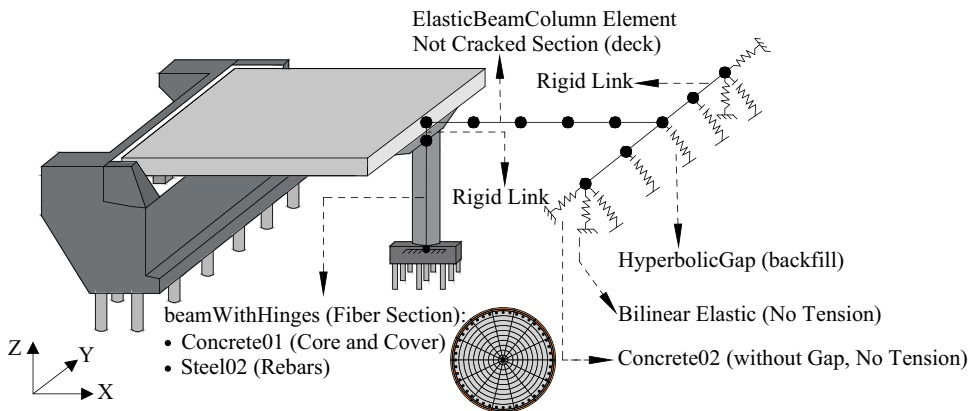


Figure 2. Illustration of the numerical modelling strategy adopted for the case study bridge, along with the pier cross-section fiber discretization.

concentrated at the two ends of the pier elements and connected by a linear elastic element with effective cross-section stiffness properties. The shear and torsional behavior of the pier was modelled elastically using a section aggregator, with the suggested stiffness reduction factors of the report of Kaviani et al. (2014). These were modelled as elastic since failure modes of this type are not expected to occur given the compliance of the case-study bridge with modern seismic design practices. The pier, pier cap and deck are constructed integrally, so a beam-type rigid link was assigned to connect the top end of the pier to the deck element. Figure 3 shows the moment-curvature response of the pier section, in addition to the lateral response of the entire element.

For what concerns the bridge ends, a simplified abutment model was adopted, where only three components were explicitly considered: (1) longitudinal response of the backfill (passive pressure) and the expansion joint; (2) transverse response of the shear keys; and (3) vertical response of the bearing pads and the stem wall. The remaining abutment components were omitted, as their contributions to the overall response have been found to be insignificant (Kaviani, Zareian, and Taciroglu 2014). Regarding the longitudinal behavior of the abutment, five springs were assigned along the deck width, all connected by a rigid beam. The soil backfill response was modelled using the *HyperbolicGapMaterial*. The strength and initial stiffness of the soil springs were obtained from the recommendations provided in Caltrans SDC (Caltrans 2010), which in turn were derived from a large-scale abutment testing (Romstad et al. 1995; Stewart et al. 2007). This material was based on abutment stiffness models for bridge simulation proposed by Wilson and Elgamal (2006) at the University of California at San Diego. The hyperbolic force-displacement model was based on work by Duncan and

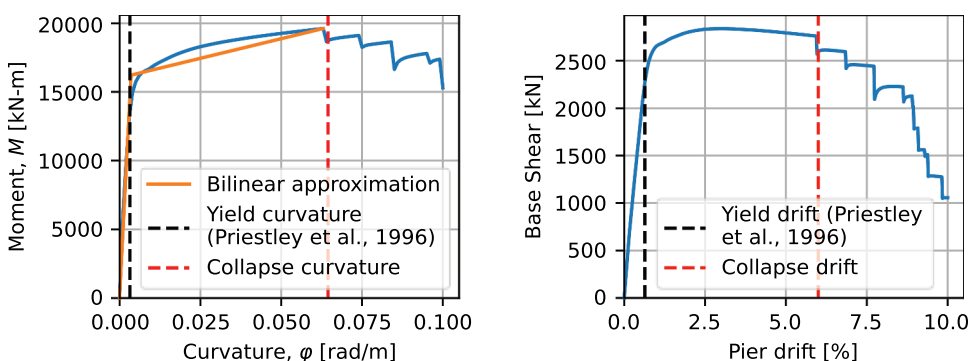


Figure 3. Moment curvature analysis and bilinearization (left). Pushover analysis of just the pier element (right).

Mokwa (2001) and Shamsabadi et al. (2007) with calibrated parameters from University of California at San Diego abutment tests. Regarding the transversal behavior of the abutment, one spring was assigned to each abutment end. It was assumed that the abutment backwall does not contribute significantly to the longitudinal load-bearing capacity of the abutment, since it fails through a brittle mechanism. The backbone curve response of the different abutment components is given in Fig. 4. Note that for each component, the response of a single spring was plotted.

Regarding the bearing pads, they were assumed to be frictionless. Thus, their transverse and longitudinal shear capacities, and generally their interaction with the deck were disregarded, except in the vertical direction. The shear keys at the deck ends were modelled using macro-elements that resist only in compression and the *Concrete02* hysteretic force-deformation model was used (Omranian et al. 2017). This hysteretic model was chosen to avoid convergence problems and solve the simultaneous parallel force balance problem by defining a small strength in tension. Further details about this bridge's characteristics and modelling assumptions are given in the "Bridge A" description of Kaviani et al. (2014). With regards to damping, a 5% tangent stiffness proportional Rayleigh damping model was applied to the first mode (Petrini et al. 2008). It should be noted that Sousa et al. (2020) suggest critical damping values ranging from 0.5% to 2% when using fiber-based elements in the model, since most of the energy-dissipation mechanisms are explicitly modeled. They also found that for these small values of critical damping, the differences between mass-proportional or tangent stiffness-proportional damping become insignificant. However, since this is a comparative study and not an explicit seismic risk assessment, it is not expected to have notable impact on the final conclusions.

Modal analysis was carried out on the bridge model and the first four modes' periods of vibration and their participating mass in each of the principal directions are listed in Table 1. As can be observed through translational and rotational modal participation factors, U and Φ , respectively, the first two modes are primarily in the X direction, with a small rotation component about the Y axis. It should be noted that these modal properties also closely match those reported by Kaviani et al. (2014) for the same bridge typology, therefore giving confidence to the accuracy and representativeness of the case study bridge model.

4. Ground Motion Records

To analyze the seismic performance of the bridge model, incremental dynamic analysis (IDA) (Vamvatsikos and Cornell 2002) was performed to characterize the non-linear dynamic response of

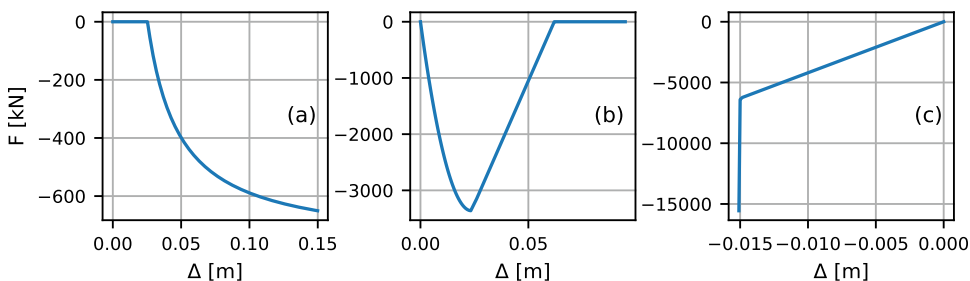


Figure 4. Backbone curve of a single abutment spring in (a) longitudinal, (b) transversal, and (c) vertical direction.

Table 1. Modal analysis results of the case study bridge.

Mode	Period [sec]	Modal participation mass ratios (%)					
		U_X	U_Y	U_Z	Φ_X	Φ_Y	Φ_Z
1	0.604	48.5	0	0	0	31.1	0
2	0.363	50.5	0	0	0	34.6	0
3	0.352	0	88.3	0	0.5	0	0
4	0.336	0	0	75.4	0	0	0

the bridge model right up to lateral collapse. To do this, a sufficiently large set of suitable ground motion records was needed to characterize the structure's seismic response adequately and to ensure an accurate marginal distribution of IM for a given EDP threshold (i.e. fragility curves). A set of 200 unscaled ground motion records from shallow crustal earthquakes were selected from the NGA West2 database (Ancheta et al. 2013) based on a scenario of magnitude, $M_w = 7.5 \pm 0.5$, rupture distance, $R_{rup} = 20 \pm 20$ km and soil conditions, $V_{s,30} = 400 \pm 300$ m/s. Out of those 200 ground motions, the 60 were classified as pulse-like records, and in 57 of them the pulse was caused due to directivity effect. The ground motion directivity effect describes how the intensity and duration of ground shaking can vary depending on the orientation of the earthquake source relative to a particular site. As seismic waves radiate outward from the fault, the ground motion can be stronger in the direction of the rupture and weaker in the opposite direction. This is not to be confused with ground motion directionality, which is a broader term and encompasses the idea that ground shaking can vary depending on the direction from which seismic waves approach a location. Regarding the fault mechanism, 84 records were caused from strike-slip, zero records from normal and 116 records from reverse faulting. A relatively large number of ground motions was chosen so that the accuracy of seismic demand estimates doesn't affect the final results and conclusions, which has been studied in the past by Sousa et al. (2016), for example. Also, a quite intense scenario was chosen to minimize the level of scaling required to bring the structure to its collapse limit. This was especially the case since the bridge under consideration was well designed against seismic actions. Table 2 reports the minimum, median, and maximum values of the IMs considered in the general sufficiency and efficiency checks, which are presented further below. It should be noted that only the horizontal components of the ground motions were applied to the structure as the bridge was not expected to be susceptible to adverse vertical ground-motion effects. Regarding the application of the ground motion records to the structure, the 1st as-recorded component in the NGA-West2 database was applied to the X (longitudinal) direction of the bridge and the 2nd as-recorded component was applied in the Y direction. This was kept constant throughout the analysis since past work (Giannopoulos and Vamvatsikos 2018) has shown that using an adequately large set of ground motion records is more important and produces more reliable results than a smaller set with varying orientation of each individual ground motion record.

5. Intensity Measures

Several studies have focused on investigating IM performance in bridge structures (Abarca et al. 2023; Avşar and Özdemir 2013; Mehdizadeh, Mackie, and Nielson 2017; Monteiro et al. 2019; O'Reilly 2021) but are typically related to the spectral acceleration-based IMs. Qian and Dong (2020) employed a novel multi-criteria decision-making approach to rank the acceptability of each alternative IM, based on holistic acceptability indices, for different structural components of a case study highway bridge. Many studies have shown how additional considerations are needed for IM selection for bridges compared to buildings. However,

Table 2. Minimum, median, and maximum values of IMs considered in the general sufficiency and efficiency checks.

$Sd_{i,RotD50}$ ($R = 2, T_1$)		$Sd_{i,RotD50}$ ($R = 3, T_1$)		$Sd_{i,RotD50}$ ($R = 4, T_1$)		$Sd_{i,RotD50}$ ($R = 6, T_1$)	
min	0.435 cm		0.519 cm		0.495 cm		0.557 cm
median	3.387 cm		3.626 cm		4.153 cm		5.512 cm
max	13.731 cm		24.753 cm		37.011 cm		55.693 cm
	$Sa(T_1)$	$Sa(1s)$	PGA	PGV	PGD	FIV3	AvgSa2
min	0.046 g	0.024 g	0.032 g	5.319 cm/s	0.397 cm	4.425 cm/s	0.046 g
median	0.380 g	0.261 g	0.185 g	37.367 cm/s	25.973 cm	62.365 cm/s	0.334 g
max	1.632 g	1.173 g	0.768 g	256.620 cm/s	365.920 cm	217.256 cm/s	1.333 g

none of these studies has so far examined the relative performance of inelastic spectral displacement-based IMs, which have been the focus of recent research (Aristeidou, Tarbali, and O'Reilly 2023; Bahrampour et al. 2023; Heresi, Dávalos, and Miranda 2018). Also, the issues of directionality are worth exploring for what concerns bridge structures and are thus examined further here.

Based on the above considerations and also the past literature on this topic for bridge structures, the following intensity measures were identified and are defined as follows:

- PGA: peak ground acceleration;
- PGV: peak ground velocity;
- PGD: peak ground displacement;
- $Sa(T_1)$: 5%-damped spectral acceleration at the fundamental period, T_1 , of the structure;
- $Sa(1s)$: 5%-damped spectral acceleration at period equal to 1 s;
- $Sd_{i,RotDnn}$: 5%-tangent-stiffness damped inelastic spectral displacement, where two *RotDnn* definitions were considered: the 50th and 100th percentile of all rotation angles sorted by amplitude (i.e. *RotD50* and *RotD100*) as defined by Boore (2010);
- FIV3: filtered incremental velocity, as defined by Dávalos and Miranda (2019) and Eq. (1);
- AvgSa: average spectral acceleration as defined by Eq. (3), which was further subdivided according to the period range as follows:
 - (a) AvgSa1 – $T \in [0.5T_1, 1.5T_1]$
 - (b) AvgSa2 – $T \in [0.5T_1, 2T_1]$
 - (c) AvgSa3 – $T \in [0.5T_1, 3T_1]$

$$FIV3 = \max\{V_{s,max1} + V_{s,max2} + V_{s,max3}, |V_{s,min1} + V_{s,min2} + V_{s,min3}|\} \quad (1)$$

$$V_s(t) = \left\{ \int_t^{t+\alpha \cdot T_n} \ddot{u}_{gf}(\tau) d\tau, \forall t < t_{end} - \infty \cdot T_n \right\} \quad (2)$$

where $V_s(t)$ is a series of incremental velocities, IVs , computed using time segments with duration $\alpha \cdot T_n$ via Eq. (2), $V_{s,max1}$, $V_{s,max2}$, and $V_{s,max3}$, are the three local maxima IVs in $V_s(t)$ and $V_{s,min1}$, $V_{s,min2}$, and $V_{s,min3}$, are the three local minima IVs in $V_s(t)$, T_n corresponds to the fundamental period of vibration of the structure, t_{end} corresponds to the last instant of time of the acceleration time series, and \ddot{u}_{gf} corresponds to the filtered acceleration time series using a second-order Butterworth low-pass filter with a cut-off frequency, f_c , equal to $\beta \cdot f_n$, where β is a scalar input that controls the f_c/f_n ratio. Dávalos and Miranda (2019) presented FIV3 as a novel IM that produced promising results for the collapse assessment of buildings. The α and β input parameters required to calculate Eq. (1) were chosen as 0.7 and 0.85, respectively, as initially proposed by the same study. However, further optimization of these parameters for bridges may be investigated in future work.

Average spectral acceleration, $AvgSa$, is another candidate included in this study for comparison. It is defined as the geometric mean of N -number spectral accelerations at periods within a user-specified range $[T_{lower}, T_{upper}]$, expressed as in Eq. (3). Different period ranges can be chosen for the definition of this IM depending on the structure and the level of inelasticity that one wants to capture more accurately. This ambiguity was investigated in several past works (Cordova et al. 2000; Vamvatsikos and Cornell 2005) and also an extensive analysis is conducted in Chapter 7 of Eads and Miranda (2013), where it was explored how the range, number, and spacing of periods used to compute $AvgSa$ influences the efficiency of collapse risk assessment estimates of single-degree-of-freedom (SDOF), moment-resisting frames, shear wall, and reinforced concrete systems. To define $AvgSa$, ten periods (i.e. $N = 10$) equally spanning each chosen period range were used as per Eq. (3). These alternative

period ranges were examined as a simple parametric study to investigate where alternative condition period ranges could improve the IMs performance in this ad-hoc case.

$$\text{AvgSa} = \left[\prod_{i=1}^N \text{Sa}(T_i) \right]^{1/N} \quad \text{for } T \in [T_{lower}, T_{upper}] \quad (3)$$

The spectral acceleration at the first mode period has been used in countless studies in recent decades for a variety of bridge structural typologies (Gardoni, Der Kiureghian, and Mosalam 2002; Mangalathu et al. 2017). Recent work by O'Reilly (2021) has discussed how the first mode period of bridge structures is generally not the dominant mode, and anchoring this IM definition to this period may not be the best solution. In fact, HAZUS (2003) recommends using Sa at period of 1 s, which is not linked directly to the bridge modal properties. Regarding the component definition of $\text{Sa}(T_1)$, the RotD50 horizontal component definition was adopted, unless otherwise stated.

The calculation of $Sd_{i,\text{RotDnn}}$ was based on a bilinear SDOF system with positive strain hardening ratio of 3%, with non-degrading and non-evolutionary hysteretic behavior. To fully define the inelastic system, the elastic period, T , and the strength ratio, also known as force reduction factor, R , are needed. The latter was defined as the ratio of maximum spectral demand in the elastic system, to the SDOF yield strength. The set of elastic periods considered was $T = [0.04, 0.06, 0.1, 0.2, 0.3, 0.5, 0.75, 1, 1.5, 2, 3, 4, 5]$ in seconds, and the set of strength ratios was $R = [1.5, 2, 3, 4, 6]$. For the calculation of the different horizontal component definitions, the ground motions were rotated from 0° to 180° with an increment of 6° and recording the maximum response for each ground motion at each rotation angle. More details on the methodology and the definition of SDOF system are given in Aristeidou et al. (2023). The horizontal component definitions examined here are the RotD50 and RotD100 definitions. The RotD50 definition was used as more recent GMMs in the NGA-West2 project have opted to use this horizontal component definition (Bozorgnia et al. 2014), while the RotD100 component was chosen because it represents the spectral maximum over all rotation angles and has been used in other models (Shahi and Baker 2014). For each IM the horizontal component definitions of geometric mean, RotD50 and RotD100 were examined and will be compared later in Section 6.2.1.

As Bradley (2012) and others have shown, an IM is the interface variable connecting seismological and engineering aspects in seismic analysis. Seismologists employ seismic hazard analysis to determine the probability of exceeding an intensity level for a certain site over a given period of time. Engineers then utilize this IM to examine the structural response and determine the seismic risk performance of a structure. This characterization of the interface IM between seismology and engineering is meant to avoid associating the structural response to rupture parameters, r_{up} , such as magnitude and distance, condensing all pertinent information in the chosen IM for engineering evaluation. To achieve this disassociation of structural response to r_{up} parameters to the highest degree possible, the IM needs to be (i) practical in its predictability via GMMs used in hazard analysis, (ii) efficient in its prediction of structural response, (iii) sufficient with respect to the underlying seismic hazard and site characteristics and (iv) unbiased with respect to other ground motion parameters and other unconditioned IMs.

For an IM to be practical, GMMs should be readily available to conduct a seismic hazard analysis for it. This can sometimes restrict the IM choice in seismic risk analysis since research has traditionally focused on peak ground acceleration/velocity/displacement and (pseudo) spectral accelerations. For these IMs, one can choose from a plethora of well-established GMMs, such as Campbell and Bozorgnia (2008), for example, which can predict all of them. For the more recently proposed FIV3, the GMM of Dávalos et al. (2020) can be utilized. A newly developed GMM also exists for the novel $Sd_{i,\text{RotD50}}$ (Aristeidou, Tarbali, and O'Reilly 2023) being evaluated as part of this study. Regarding AvgSa, the logarithmic mean and variance for a given rupture scenario can be computed either directly using a GMM (Dávalos and Miranda 2021; Kohrangi, Kotha, and Bazzurro 2018), or indirectly utilizing the $\text{Sa}(T)$ values given by other GMMs (Kohrangi et al. 2017).

Efficiency means that the structural response, measured by an EDP, should exhibit low record-to-record variability at any given level of the IM, or reversely low IM level variability at any given structural response (EDP) level. This IM attribute allows one to accurately evaluate the conditional EDP distribution with relatively few response-history analyses. This can become important when conducting numerous non-linear dynamic analyses for a building class portfolio or in regional assessment. However, it is worth noting that within a risk assessment framework, like the PEER-PBEE framework (Cornell and Krawinkler 2000), this reduction in response dispersion gained by a more efficient IM, does not necessarily reduce the overall dispersion. A more efficient IM may be more structure-specific and, therefore, present lower EDP dispersion, $\beta_{EDP|IM}$, but this may come at the cost of higher dispersions when defining an appropriate GMM, $\beta_{IM|rup}$ (Kohrangi et al. 2017). Therefore, the eventual risk metric may still result in a high dispersion. This issue is briefly examined in Fig. 5, where the dispersions (i.e. logarithmic standard deviations) of all the IMs are shown for demonstration purposes for the rupture scenario described in Section 4. The GMM of Campbell and Bozorgnia (2008) was used to obtain the dispersions of all spectral IMs, except FIV3 and $Sd_{i,RotD50}$, and the additional parameters needed for the model input were taken as the mean parameters of the used ground motion suite. It can be seen that all IMs, except PGD, have $\beta_{IM|rup}$ between 0.5 and 0.7. The elastic spectral values, PGA and PGV exhibit dispersions between 0.5 and 0.62, while $Sd_{i,RotD50}$ exhibit dispersions between 0.64 and 0.7, proportionally to the degree of inelasticity. Generally, it can be said that all the IMs investigated present ground motion prediction uncertainties of a similar order of magnitude, except PGD, meaning that the direct comparison of the IM's efficiency is reasonable. However, it should be noted that the logarithmic standard deviations of IMs are slightly changing from GMM to GMM.

The sufficiency criterion mandates that seismological parameters should not influence the seismic response characterized via the IM, eliminating any bias against, for example, magnitude, distance, or fault rupture mechanism. Sufficiency is deemed the most important condition of a good IM because an insufficient IM will leave the EDP response exposed to seismological parameters.

Another desirable property of an IM is for it to be unbiased. Meaning that even if the IM is efficient and sufficient, the structural response should not be impacted by any other unconditioned IM that would otherwise require particular attention during the ground motion selection process. It is similar to the sufficiency property but with other IMs instead of seismological parameters. However, it is not to say that structural response should be

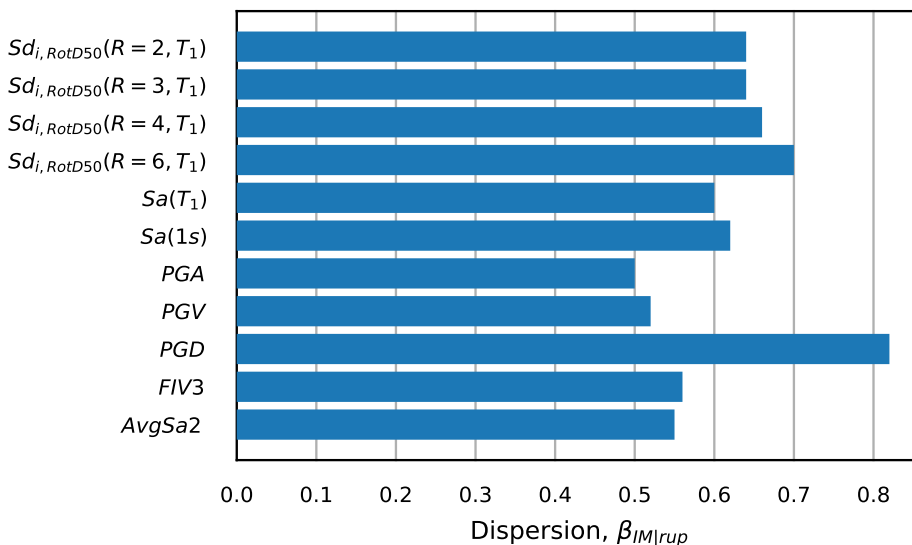


Figure 5. GMM dispersions of each IM examined for a given rupture scenario.

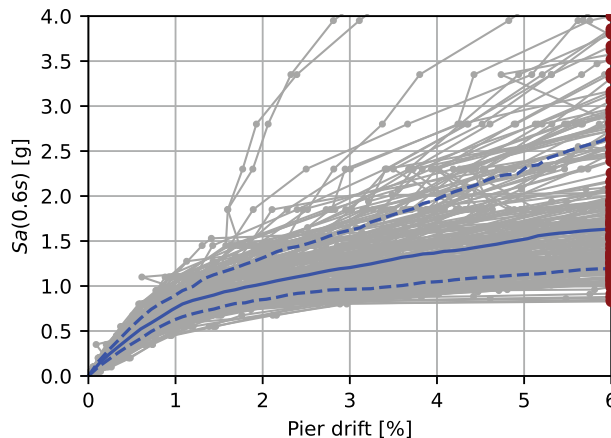


Figure 6. IDA curves with median, 16 and 84 percentiles.

independent of other IMs, as in the case of sufficiency, but rather to say that it would be desirable for the chosen IM for a specific structural typology not to be significantly impacted by other IMs not considered during the ground motion selection process. For example, for the case of non-ductile infilled frames, O'Reilly (2021) identified that using $Sa(T_1)$ as the IM results in the structural response being notably biased by the velocity-based characteristics of the ground motions used. This would mean that an analyst would need to pay particular attention to these characteristics of the IMs when using $Sa(T_1)$ and ensure that they are indeed representative. However, it was also shown that simply using AvgSa tended to remove this biasing effect, making it a much more attractive IM. The latter situation is a much simpler case to implement in practice.

6. Analysis Results

Using the set of 200 ground motion records described in Section 4, IDA was performed to quantify the complete response of the bridge structure up to collapse. For computational efficiency, this was done using the hunt and trace algorithm described in Vamvatsikos and Cornell (2002). The EDP chosen was the pier drift, and the IDA was conducted until a pier drift of 10%. The curves, however, are plotted until 6%, as this was the value at which the pier began to lose lateral strength capacity during the pushover analysis of the pier element, which is depicted in Fig. 3. The IDA was initially conducted using $Sa(T_1)$ as the IM, as shown in Fig. 6, and the IDA curves for the other IMs described in Section 5 were obtained by simple post-processing of the analysis results to allow for relative comparisons.

Figure 6 illustrates an example set of IDA curves for all ground motion records. Also plotted are the median trend of the response along with the 16th and 84th percentiles to graphically illustrate the variability of the structural response. The general trend of the median is a steady increase with intensity before reaching a plateau (i.e. flatline), where the structure is considered to be collapsed. It can be seen that the IM dispersion is relatively low initially and gradually increases. This dispersion is mainly a combined consequence of the record-to-record variability of the ground motions, the IM used and the multi-modal behavior of the inelastically responding structure. The response may also be examined in terms of alternative EDPs, for instance, the longitudinal and transversal response at the abutment system. However, these were not considered to be principal elements to examine for the purpose of the present study but whose non-linear response would nonetheless be represented in the numerical model used.

6.1. Sufficiency

As previously mentioned in Section 5, sufficiency of an IM is a fundamental property to check and verify since it must be independent of the rupture parameters that produced each ground motion and permit widespread application. Here, the sufficiency of the IMs analyzed was checked against the moment magnitude, M_w , rupture distance, R_{rup} , and level of amplitude scaling applied to the ground motions, SF . To do this, the IM levels required for each ground motion during IDA to induce collapse in the bridge structure were checked. The results of IDA were utilized to characterize the collapse intensity of the selected 200 ground motions (i.e. the red dots in Fig. 6). The residuals with respect to the logarithmic mean (assuming that the residuals follow a lognormal distribution in the considered range of IMs and EDPs) of residuals from all ground motions were examined to determine whether there was any dependency of the collapse intensities, s , on the ground motion rupture parameters. These intensity-based residuals, ε_s , were calculated as per Eq. (4) for a given ground motion i causing the collapse of the case study structure.

$$\varepsilon_{s,i} = \frac{s_i}{\bar{s}} = \frac{s_i}{\exp\left(\frac{1}{n} \sum_{i=1}^n \ln(s_i)\right)} \quad (4)$$

where n is the number of ground motions used in IDA. Note that lower values of ε_s denote more aggressive ground motion records since it means a below-average intensity ground motion was able to induce collapse. The relative trends between the collapse residuals and the ground motion parameters checked were investigated via fitting a log-linear regression trendline to the data, as shown in Eq. (5). The p values of $\beta_{1,s}$ from that regression were examined.

$$\ln(\varepsilon_s) = \beta_{0,s} + \beta_{1,s} rup \quad (5)$$

where $\beta_{0,s}$ and $\beta_{1,s}$ is the y-intercept and slope of the log-linear interpolation, respectively, and rup represents either M , R_{rup} , or SF for the scope of this study.

While there is no common consensus on the optimal metric of IM sufficiency (Luco and Cornell 2007), the most widespread is the statistical significance (i.e. p -value) of residuals with respect to the different rupture characteristics. The p -value corresponds to a test hypothesis whose null hypothesis is that the slope is zero, computed using the Wald Test with t -distribution of the test statistic. A low p -value indicates that the data do not conform to what the statistical distribution predicted they should be, which implies that the slope of the regression is probably far from zero and, therefore, there is likely some dependence on the rup parameter under evaluation. Meanwhile, a large p -value would likely indicate that the data are close to the model prediction. That is, there is probably no clear relationship between the residuals and the rup parameter. A significance threshold of 5% is typically adopted in literature and was also used here.

In addition to the common p -value, the simplified relative sufficiency (SRS) evaluation proposed by Dávalos and Miranda (2019) was also used to quantify the sufficiency. The SRS procedure entails a linear regression between the normalized collapse intensities and the ground motion parameter of interest. From that, the slope is computed and used to measure the SRS of each IM by checking how close to zero it is and by comparing it to the slope obtained from the other IMs. Slopes that are zero, or close to zero, indicate that the ground motion parameter being investigated has little to no influence on the structural response. This procedure does not classify an IM as sufficient or insufficient, as it is commonly done using an arbitrary limiting p -value in a null hypothesis test, but rather assesses the sufficiency of an IM relative to the others by using their normalized slopes as a measure of sufficiency.

By adopting these two methods of assessing IM sufficiency, Table 3 lists the p -values and the SRS slopes of each IM, with respect to magnitude, rupture distance and scale factor. By visual inspection of Fig. 7a-c, it can be inferred that almost no IM presents an obvious case of insufficiency with respect to any of the parameters investigated. The only exception is the PGA residuals versus the SF in Fig. 7c, where the slope is disproportionately higher compared to the other IMs. It was speculated that data with high scale factors may disproportionately influence the calculated slopes and therefore the eventual

**Table 3.** *P*-values and SRS slopes for the IDA residuals for each IM and parameter investigated.

Intensity measure	p-values			SRS slopes		
	M_w	R_{rup}	SF	M_w	R_{rup}	SF
$Sd_{i,RotD50} (R = 2, T_1)$	0.004	0.193	$<10^{-3}$	-0.248	0.003	0.018
$Sd_{i,RotD50} (R = 3, T_1)$	0.147	0.622	$<10^{-3}$	-0.111	0.001	0.013
$Sd_{i,RotD50} (R = 4, T_1)$	0.437	0.566	0.031	0.059	-0.001	0.008
$Sd_{i,RotD50} (R = 6, T_1)$	0.001	0.257	0.670	0.324	-0.003	0.002
$Sa(T_1)$	$<10^{-3}$	0.248	$<10^{-3}$	-0.365	0.003	0.019
$Sa(1s)$	0.193	0.407	0.355	-0.075	-0.001	0.004
PGA	$<10^{-3}$	0.250	$<10^{-3}$	-0.729	0.004	0.050
PGV	0.218	0.117	$<10^{-3}$	0.096	-0.003	0.014
PGD	$<10^{-3}$	0.204	0.663	0.581	-0.005	0.004
FIV3	$<10^{-3}$	0.349	0.351	0.161	0.001	0.002
AvgSa2	$<10^{-3}$	0.264	$<10^{-3}$	-0.318	0.002	0.017

results. This was checked by eliminating data with scale factors higher than 20 and calculating again the slopes and p-values, where it was found that the ranking of IMs remained the same. Hence, while it is an important issue to check and scrutinize, it does not impact the conclusions. A clearer comparison can be made from the sufficiency metrics listed in Table 3. It can be observed that $Sd_{i,RotD50}$ with $R = 3$ and 4, $Sa(1s)$ and PGV have *p*-values above the threshold of 5%, meaning that the observed data pass the test hypothesis prediction and therefore are independent of M . The rest of the IMs cannot be deemed independent of M from this test. This does not necessarily mean that they are insufficient, but instead that the test cannot provide a decision on whether they are sufficient or not. With respect to R_{rup} , all IMs can be considered statistically independent from it since they all result in *p*-values greater than 5%. With respect to SF, only $Sd_{i,RotD50}$ with $R = 6$, $Sa(1s)$, PGD and $FIV3$ can be deemed statistically independent. Examining the SRS, however, provides more intuitive guidance on the sufficiency of these IMs. Regarding the second sufficiency metric (i.e. SRS slope), it seems that $Sd_{i,RotD50}$ with $R = 4$, $Sa(1s)$ and $FIV3$ perform the best across all the *rup* parameters examined. It should be stated that with both methods of assessing IM sufficiency (i.e. *p*-values and SRS slopes), a major issue is that a poor regression may influence the results. Therefore, a non-regression approach to examine sufficiency such as that utilized by Kazantzi and Vamvatsikos (2015) may be a better alternative.

6.2. Efficiency

Considering the IDA response in Fig. 6 for the case study bridge structure, the efficiency of the IMs was examined. This was done by examining the relative dispersion in the results to evaluate each IM's predictive power. A principal assumption is that the data shown in Fig. 6 are lognormally distributed and characterized by a median and dispersion value pair, $\{\eta, \beta\}$. For the present study, the dispersion of IM at a given EDP, $\beta_{IM|EDP}$, also known as record-to-record variability, β_{RTR} , was computed for each IM examined over an EDP range, as initially carried out by Vamvatsikos and Cornell (2005). The dispersions for each IM described previously in Section 5 were computed and are depicted in Fig. 8. Also shown is the corresponding pier displacement ductility, μ_Δ , where it can be seen that a ductility well over 8 was obtained before the lateral collapse of the pier element.

Beginning with the spectral acceleration, it can be seen how $Sa(T_1)$ gives relatively low dispersion in the elastic range (i.e. $\mu_\Delta < 1$) and close to it, but the dispersion increases significantly as the structure goes well into the non-linear range of response. This is an expected result for any structure since past studies (Bradley et al. 2009; Haselton and Baker 2006; T. Lin, Haselton, and Baker 2013; Shome et al. 1998) have shown that $Sa(T_1)$ is well correlated with deformation-based EDPs for first-mode-dominant structures. $Sa(1s)$ presents poor efficiency in the initial elastic and inelastic stages but gets progressively better with displacement ductility and is classified as

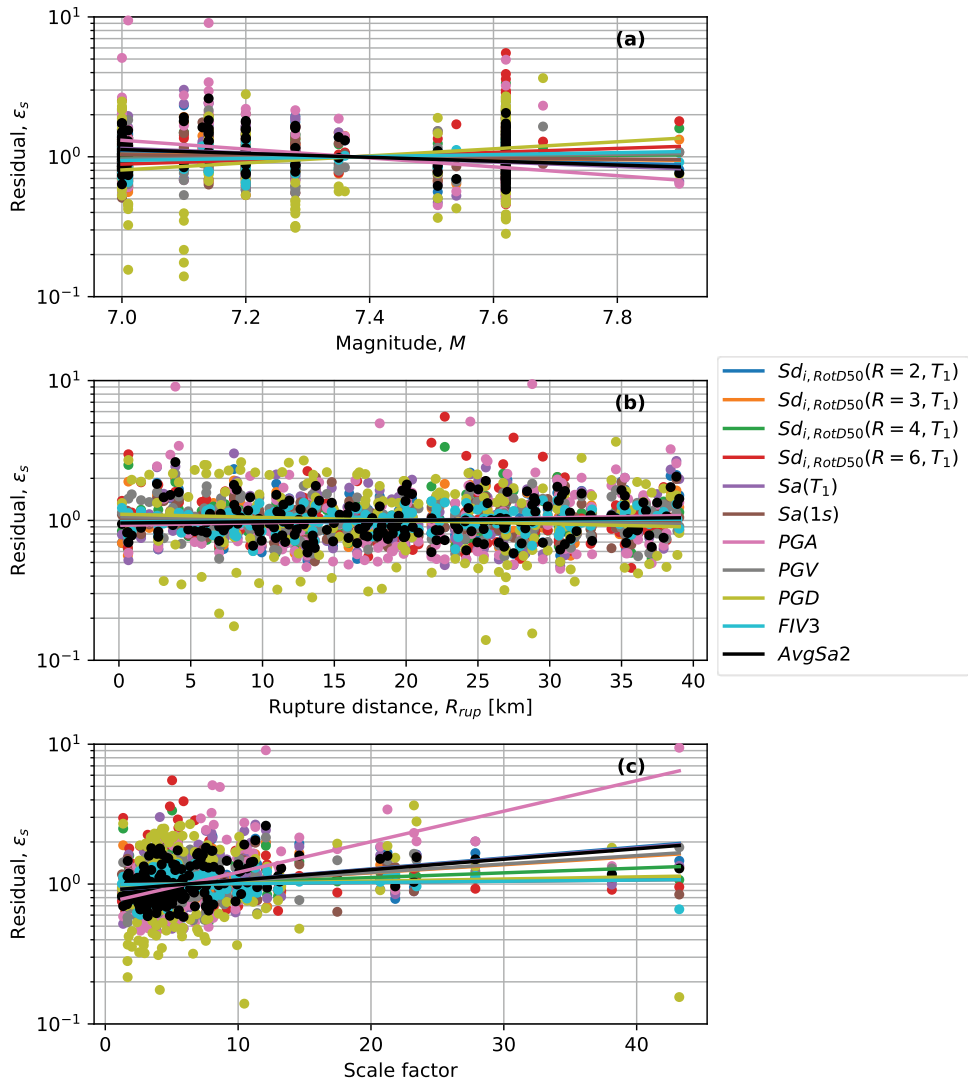


Figure 7. Observed trends of IM residuals versus each ground motion parameter investigated. (a) magnitude; (b) rupture distance; (c) scale factor applied during IDA.

the second most efficient IM in the collapse limit. PGD exhibits the highest $\beta_{IM|EDP}$ throughout the whole range of structural response, whereas PGA is also seen to increase progressively, making them the worst performers among all IMs.

Meanwhile, in the region with a highly inelastic response and near the collapse limit it is the $FIV3$ which performs the best. This result supports the findings of the original study that proposed this IM (Dávalos and Miranda 2019). Specifically, this IM has demonstrated the highest efficiency in predicting the seismic collapse intensities of the structure, as evidenced by the smallest record-to-record variability. This effect of $FIV3$ is because, unlike other IMs based on the peak response of one or more linear elastic oscillators, it is defined based on features of severe long-duration acceleration pulses present in the acceleration time series, which are deemed to be the main drivers of collapse.

Among the novel $Sd_{i,RotD50}$ definitions, the most efficient for pier drifts lower than about 3% is the one with $R = 2$, whereas for drifts higher than 3% $R = 3$ performs better. This is expected, since the force reduction factor of the SDOF, with which $Sd_{i,RotD50}$ was developed, is a proxy of the inelasticity

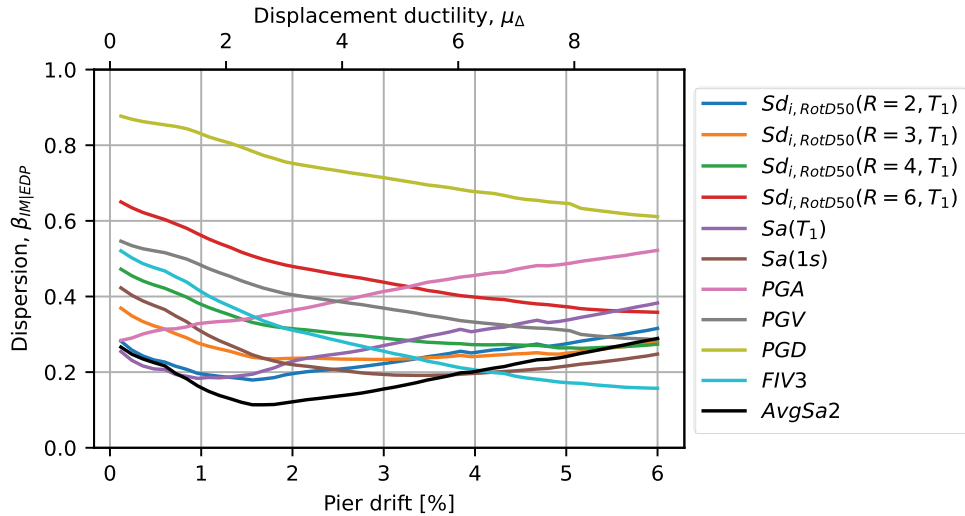


Figure 8. Dispersion versus pier drift and displacement ductility for each IM investigated.

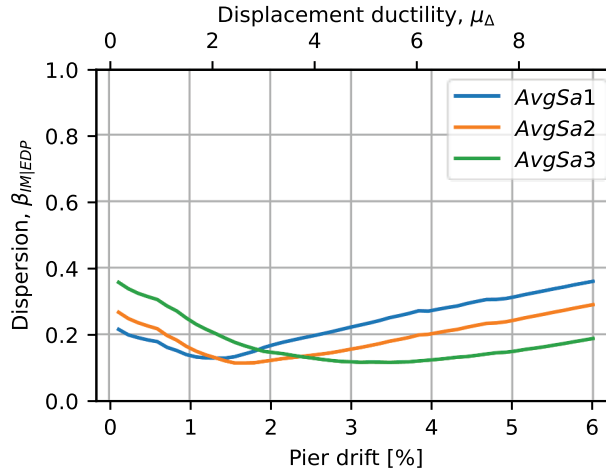


Figure 9. Marginal dispersion of $AvgSa$ with different period ranges.

that the system is expected to undergo. Ergo, a higher R corresponds to higher efficiency in the high EDP region.

The dispersion of the three definitions of $AvgSa$ investigated was calculated and plotted in Fig. 9 for the whole range of non-linear responses. The lower bound of the period range was kept the same since it was seen that the dispersion was already low enough for low EDP values. It can be seen that $AvgSa1$ performs the best for pier drifts until about 1.3%, then for drifts of 1.3–2.3%, the $AvgSa2$ is the most efficient and from there until 6% drift the $AvgSa3$ has the best performance. This is expected since the upper bound of the period range accounts for the effects of period elongation during non-linear response. Therefore, the structural response deep into the non-linear range is better explained using a higher T_{upper} . Taking $AvgSa2$ to be the best overall performer for the case study presented here, it can be seen from Fig. 8 that it is the most efficient IM in the initial elastic region and, most evidently, in the intermediate inelastic region.

From these observations, it is clear that the choice of IM depends on which part of the structural response is of interest, as no single IM produces the overall best efficiency. For example, if an

inefficient IM, such as PGD , PGA , or $Sa(T_1)$, is chosen to estimate the IM at the collapse limit state, it will result in high dispersion in the results and require many more ground motion records to characterize the collapse fragility sufficiently. However, some of these IMs work better at limit states other than collapse. Importantly for what concerns the main aim of this study is that the inelastic spectral displacement definitions of IM have shown promising performance as IMs, with comparable, if not better, efficiency with respect to other notable IMs currently in use. The recent development of a GMM and its anticipated implementation into hazard analysis tools such as OpenQuake means that it is also quite a practical IM to use.

6.2.1. Comparison of Different Horizontal Component Definitions

While the previous section looked at the relative efficiency of the different IMs, this section looks at the impacts the horizontal component definition can have on these results. To do this, the efficiency of three horizontal component definitions of elastic spectral accelerations and inelastic spectral displacements were examined. The results of the relative comparison are shown in Fig. 10.

It was calculated that the dispersion in the $RotD100$ component definition of the $Sa(T)$ is around 8.1% higher on average than the $RotD50$ component. This is a somewhat expected result when considering the actual definition of these IMs: the $RotD50$ component is the median over all directions; hence, it has a more averaging effect and does not suffer from peaks as much as the $RotD100$ component does, since it takes the maximum over all directions. The same observation is also noted for the $AvgSa$ shown in Fig. 10(a), but with a less amplified effect as it is only 2.9% higher on average, likely because of the further averaging effect of $AvgSa$ over the predefined period range. The geometric mean definition gives very similar values of dispersion with the $RotD50$ definition for elastic spectral accelerations. Specifically, for pier drift lower than about 2% the geometric mean gives slightly higher dispersions, whereas for pier drift higher than about 2% it gives slightly lower dispersions. These trends are more apparent in the case of $Sa(T)$ rather than $AvgSa$.

Regarding the inelastic spectral displacement IMs, Sd_i , the same general trend is observed as in the case of the other IMs, which is conceptually consistent. However, it is worth noting that the ratio of the dispersions between the $RotD100$ and $RotD50$ definitions is larger, around 17.3% on average. This is because inelastic spectral displacement is used as the IM, where the non-linear cycles produce a maximum displacement that can accumulate more displacement in the non-linear range; hence, the maximum with respect to the median definitions can tend to deviate more, as observed in Fig. 10(b). From a visual inspection of Fig. 10(b), this may be the case, but no significant trend is noted, as the average ratios are 10.7%, 23.3%, 22.2% and 13.0% for the $R = 2, 3, 4$ and 6 cases, respectively. Strangely enough, the highest ratios of dispersion are observed for the intermediate

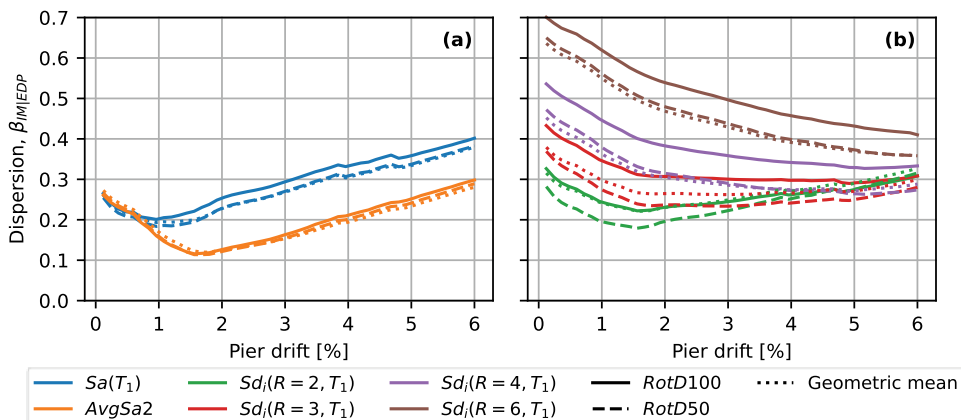


Figure 10. Comparison of dispersion for different horizontal component definitions (a) elastic spectral accelerations and (b) inelastic spectral displacements.



R factors, hence there is not an evident trend among the different Sd_i definitions. The geometric mean definition gives generally lower dispersions than $RotD50$ for the Sd_i with high inelasticity (i.e. $R = 6$ and 4) and higher dispersions for the Sd_i with lower inelasticity (i.e. $R = 2$ and 3).

6.3. Bias Against Directionality

In the previous sections, the focus was solely on the ability of scalar IMs to accurately characterize the non-linear response. Nevertheless, part of that observed record-to-record variability can be explained by separate pertinent but unconditioned ground motion characteristics biasing the response. This hidden bias from different ground motion characteristics (e.g. duration) can introduce a large scatter in the eventual structural response data (e.g. collapse intensities) if not considered properly in the record selection process (Chandramohan, Baker, and Deierlein 2016). Ground motions selected and scaled to a single conditioning IM, denoted as IM_j here, could depend on, or be biased by another IM, denoted as IM_i . However, this poses no problem if both IM_j and IM_i are consistent with, or match, the site hazard curves obtained from probabilistic seismic hazard assessment (PSHA) (Bradley 2010), which could be cumbersome to take care of in a common performance-based seismic assessment.

In this section, it was investigated whether the ground motion directionality is influencing the sufficiency of the IMs examined here. This was done by checking whether IM_j exhibits any notable statistical dependence on IM_i parameters. The IM_i parameters chosen to represent directionality were the $Sa_{RotD100}/Sa_{RotD50}$ for the elastic case and $Sd_{i,RotD100}/Sd_{i,RotD50}$ for the inelastic case, denoted for brevity as κ and κ_i , respectively. Should a bias be found, it means that the effect of directionality on structural response is not negligible. Due to the format of the analysis (i.e. IDA) the bias was examined upon the collapse cases, where the collapse intensity residuals, ε_s , were used similarly to what was done to check sufficiency in Section 6.1. The same functional form of Eq. (5) was used, but the r_{up} is now replaced by the term $\ln(IM_i)$. For each IM_j , the collapse intensity residuals were computed as previously described in Eq. (4). The linear trend was fitted using least squares regression. The slopes obtained from each IM_i were graphically examined and compared. The same hypothesis test of $\beta_{1,s} = 0$, which was previously used, can be used again here, to gain some insight on the statistical significance between the collapse intensities and directionality measures. A low p -value (i.e. <0.05) would suggest that the influence of directionality on collapse capacity is statistically significant. Another relative comparison between the different IMs is simply comparing the slope, $\beta_{1,s}$, of different IM_i and IM_j pairs. These assessment metrics are considered to be theoretically sound, since, in principle, there should not be any notable correlation between $Sa(T_1)$ and κ or κ_i , meaning that a record causing collapse with a certain value of $Sa(T_1)$ does not convey almost any information regarding the directionality of the record.

From Fig. 11 it can be observed that the collapse residuals of all IM_j are completely independent of κ . However, when the inelastic directionality ratio is used as a metric of ground motion directionality there is an apparent dependency. In other words, ε_s is biased from κ_i , but not from κ , which may be an indicator that the newly proposed directionality measure can be a better proxy to describe the ground motion directionality characteristics rather than the classic elastic κ . There is a negative trend slope of residuals of $Sa(T_1)$, $AvgSa$ and PGA with κ_i , while for the Sd_i it gets from negative to positive for $R = 2$ to $R = 6$, respectively. PGV , PGD and $FIV3$ residuals seem to be unaffected by the degree of inelastic directionality since the slope of their trend lines is close to zero. In order to check for possible issues of linear regression when outliers are present, only κ_i values lower than 2 were kept and the calculations were performed again and shown in Fig. 12. It can be seen that the relative slopes between the IMs stay about the same, but the absolute slopes become lower and therefore less significant. This suggests that the outliers (i.e. ground motions with high inelastic directionality) are influencing the degree of bias seen in Fig. 11.

Figure 13 confirms that $Sa(T_1)$ collapse intensities are not influenced by κ , where the p -value of 7.4% suggests statistical insignificance (i.e. $>5\%$) and the low coefficient of determination, R^2 , (0.02) indicates that the collapse intensities cannot be explained from κ . The R^2 statistic is a measure of the

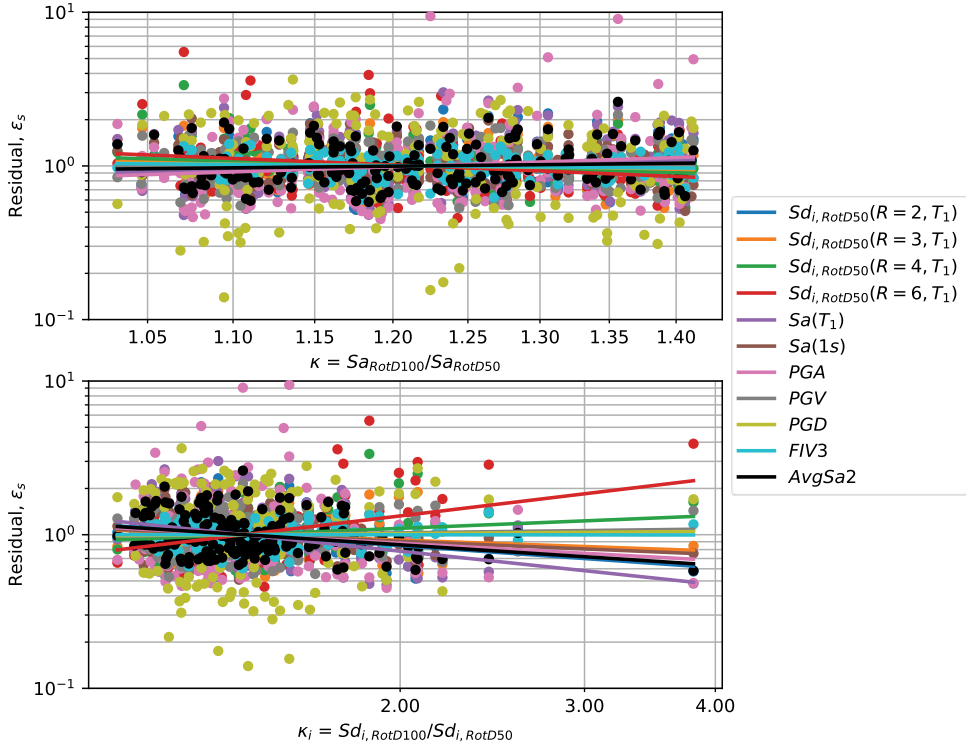


Figure 11. Trends of collapse IM residuals versus elastic and inelastic directionality measure. For the $Sd_{i,RotD100}/Sd_{i,RotD50}$, R equal to 3 was used.

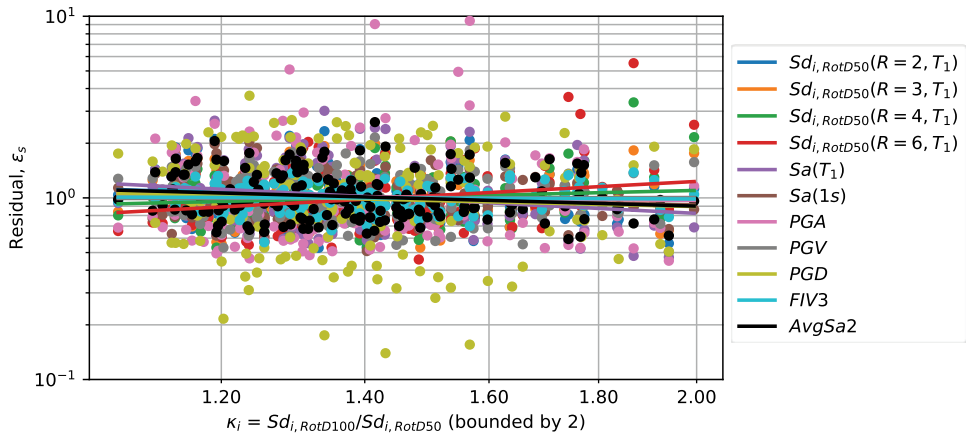


Figure 12. Trends of collapse IM residuals versus the inelastic directionality measure, $Sd_{i,RotD100}/Sd_{i,RotD50}$, with R equal to 3. Only values of κ_i below 2 are kept.

capability of $\ln(IM_i)$ to predict the $\ln(IM_j|\text{collapse})$. Meanwhile, collapse intensities are plotted against the κ_i with different strength ratios, R , in Fig. 14. It can be visually observed that the $Sa(T_1)$ are somewhat biased by κ_i , which is also indicated by the slope of the trend line, the low p -values ($<5\%$) and higher R^2 values. Comparing the κ_i with different R ratios, the steepest slope is found for $R = 2$, and the lowest for $R = 4$. It can be concluded from the negative trend line slope that, on average, the higher the κ_i , the lower the expected collapse capacity the structure would be expected to exhibit. All in all,

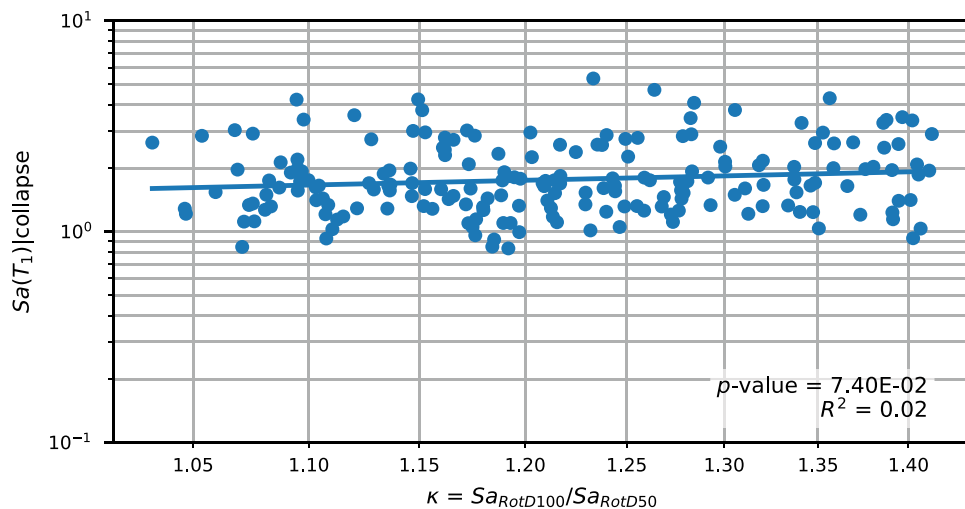


Figure 13. Collapse $Sa(T_1)$ intensities versus the elastic directionality measure, κ , along with the fitted linear trend line.

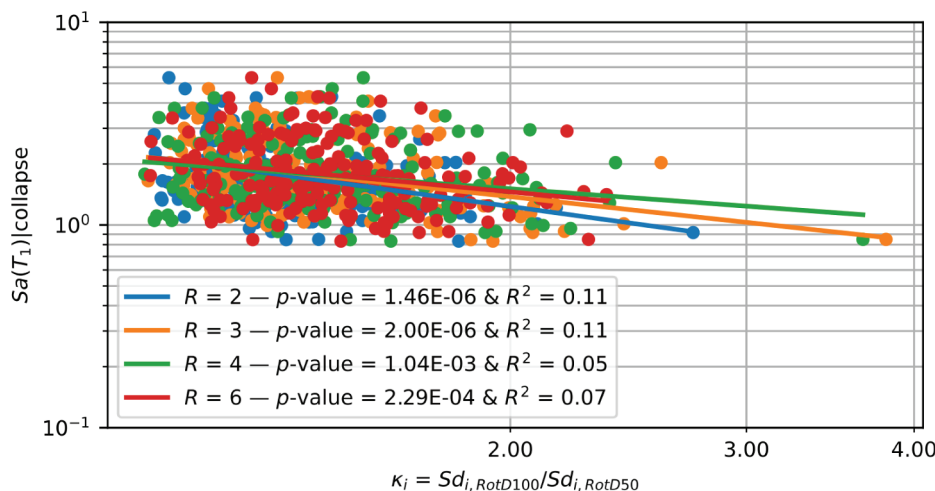


Figure 14. Collapse $Sa(T_1)$ intensities versus the inelastic directionality measure, κ_i , with different strength ratios, R .

this means that this IM_i is a good secondary predictor of the intensity of ground motions, independently of elastic spectral values. Lastly, to check the degree to which the outliers are influencing the regression and consequently the bias results, κ_i values up to 2 were considered. In that evaluation, the slope ranking did not significantly change, the p-values were ranging from 0.0395 to $3.36 \times 10^{(-5)}$, and the R^2 from 0.02 to 0.09 . Ultimately, it was decided that the outliers do not significantly affect the bias results and only the complete set of data was presented here.

7. Summary and Conclusions

This paper has investigated the use of inelastic spectral displacements, Sd_i , as an intensity measure (IM) for the seismic assessment of bridge structures. A typical reinforced concrete highway bridge in California was employed for the case study comparisons and its dynamic response up to collapse was

characterized by the ground shaking intensity. A number of traditional and modern IMs were examined and compared on the basis of their efficiency and sufficiency. Based on the outcomes of this study, the following conclusions can be summed up:

- The novel IM $Sd_{i,RotD50}$ performed relatively well in predicting the EDP, both under efficiency and sufficiency checks. An interesting and expected result is that the efficiency of Sd_i with different force reduction factors, R , varies with the level of inelasticity. Specifically, for low R factors, the lowest dispersions are found in the elastic or early inelastic ranges, whereas for the higher R factors, the lowest dispersion are found deeper into the inelastic range or near the collapse limit;
- For the widest range of structural response, it was the $AvgSa_2$ that was the most efficient (i.e. displayed the lowest dispersion). The period range used to define $AvgSa$ can have a significant impact. It depends on which level of inelastic response the best control over is required for;
- Regarding the sufficiency of IMs checked on the collapse limit, it was found that $Sd_{i,RotD50}$ ($R = 4$, T_1) and $FIV3$ were the most sufficient of the IMs examined. This is concluded by taking into account all the comparative metrics of sufficiency employed herein;
- The $RotD100$ component falls short in its predictive power of the resultant pier drift response compared to the $RotD50$ component. This is the case for both elastic and inelastic spectral values, with the effect on inelastic spectral values being more amplified.
- An apparent bias of collapse $Sa(T_1)$ intensities was observed against the inelastic directionality measure, but not against the elastic one. The results indicate that the inelastic directionality measure recently developed by the authors is a more comprehensive way to classify the ground motion directionality, rather than the elastic one.

Nomenclature

$AvgSa$	average spectral acceleration
EDP	engineering demand parameter
f_c	cut-off frequency of second-order Butterworth low-pass filter
$FIV3$	filtered incremental velocity
f_n	natural frequency
GMM	ground motion model
IDA	incremental dynamic analysis
IM	intensity measure
IVs	incremental velocities
M_w	moment magnitude
N	Number of spectral accelerations used for the calculation of average spectral acceleration
PBEE	performance-based earthquake engineering
PGA	peak ground acceleration
PGD	peak ground displacement
PGV	peak ground velocity
PSHA	probabilistic seismic hazard assessment
R	strength ratio, also known as force reduction factor
R^2	coefficient of determination
$RotDnn$	nn^{th} fractile of a response spectral value for all rotation angles sorted by amplitude
R_{rup}	rupture distance
rup	ground motion rupture parameter
\hat{s}	logarithmic mean of collapse intensities from all the ground motions
$Sa(T)$	spectral acceleration at period T
$Sd_{i,RotDnn}$	nn^{th} percentile of all rotation angles of the inelastic spectral displacement
SDOF	single-degree-of-freedom
SF	scaling factor
s_i	collapse intensity of the i^{th} ground motion
SRS	simplified relative sufficiency
T	oscillation period
t_{end}	last instant of time of the acceleration time series
U	translational modal participation factor



\ddot{u}_{gf}	filtered acceleration time series
$V_s(t)$	series of incremental velocities
$V_{s,30}$	time-averaged shear-wave velocity for the top 30 m of soil
$V_{s,max}$	local maximum IVs in $V_s(t)$
$V_{s,min}$	local minimum IVs in $V_s(t)$
$\alpha \cdot T_n$	time segment duration for the calculation of IV
β	scalar that controls the f_c/f_n ratio
$\beta_{0,s}$	y-intercept of the log-linear interpolation
$\beta_{1,s}$	slope of the log-linear interpolation
$\beta_{EDP IM}$	dispersion of EDP given IM
$\beta_{IM rup}$	Dispersion of IM given a set of rupture parameters
β_{RTR}	record-to-record variability
ϵ_s	collapse intensity residuals
ϵ_{su}	steel ultimate strain
κ	$Sa_{RotD100}/Sa_{RotD50}$
κ_i	$Sd_{i,RotD100}/Sd_{i,RotD50}$
Φ	Rotational modal participation factor

Acknowledgments

The work presented in this paper has been developed within the framework of the project “Dipartimenti di Eccellenza”, funded by the Italian Ministry of Education, University and Research at IUSS Pavia. The comments and feedback of Davit Shahnazaryan are also gratefully acknowledged in addition to the discussions with Karim Tarbali during the early development of this research.

Disclosure Statement

No potential conflict of interest was reported by the author(s).

ORCID

Savvino Aristeidou <http://orcid.org/0000-0002-4224-7891>
G. J. O'Reilly <http://orcid.org/0000-0001-5497-030X>

Data Availability Statement

The data and models used as part of this study will be made available upon request.

References

- Abarca, A., R. Monteiro, G. O'Reilly, E. Zuccolo, and B. Borzi. 2023. “Evaluation of Intensity Measure Performance in Regional Seismic Risk Assessment of Reinforced Concrete Bridge Inventories.” *Structure and Infrastructure Engineering* 19 (6): 760–778. <https://doi.org/10.1080/15732479.2021.1979599>.
- Abarca, A., R. Monteiro, and G. J. O'Reilly. 2022. “Simplified Methodology for Indirect Loss-Based Prioritization in Roadway Bridge Network Risk Assessment.” *International Journal of Disaster Risk Reduction* 74 (December 2021): 102948. <https://doi.org/10.1016/j.ijdrr.2022.102948>.
- Ancheta, T., R. Darragh, J. Stewart, E. Seyhan, W. Silva, B. Chiou, K. Wooddell, et al. 2013. *PEER NGA-West2 Database, Technical Report PEER 2013/03*.
- Aristeidou, S., K. Tarbali, and G. J. O'Reilly. 2023. “A Ground Motion Model for Orientation-Independent Inelastic Spectral Displacements from Shallow Crustal Earthquakes.” *Earthquake Spectra* 39 (3): 1–23. <https://doi.org/10.1177/87552930231180228>.
- Avşar, Ö., and G. Özdemir. 2013. “Response of Seismic-Isolated Bridges in Relation to Intensity Measures of Ordinary and Pulse like Ground Motions.” *Journal of Bridge Engineering* 18 (3): 250–260. [https://doi.org/10.1061/\(ASCE\)BE-1943-5592.0000340](https://doi.org/10.1061/(ASCE)BE-1943-5592.0000340).
- Bahrampouri, M., Y. Bozorgnia, S. Mazzoni, and K. Campbell. 2023. *Use of inelastic response spectra in seismic hazard analysis and design*. Los Angeles: University of California. <https://doi.org/10.34948/N38G6K>.

- Boore, D. M. 2010. "Orientation-Independent, Nongeometric-Mean Measures of Seismic Intensity from Two Horizontal Components of Motion." *Bulletin of the Seismological Society of America* 100 (4): 1830–1835. <https://doi.org/10.1785/0120090400>.
- Boore, D. M., J. Watson-Lamprey, and N. A. Abrahamson. 2006. "Orientation-Independent Measures of Ground Motion." *Bulletin of the Seismological Society of America* 96 (4 A): 1502–1511. <https://doi.org/10.1785/0120050209>.
- Borzi, B., P. Ceresa, P. Franchini, F. Noto, G. M. Calvi, and P. E. Pinto. 2015. "Seismic Vulnerability of the Italian Roadway Bridge Stock." *Earthquake Spectra* 31 (4): 2137–2161. <https://doi.org/10.1193/070413EQS190M>.
- Bozorgnia, Y., N. A. Abrahamson, L. Al Atik, T. D. Ancheta, G. M. Atkinson, J. W. Baker, A. Baltay, et al. 2014. "NGA-West2 Research Project." *Earthquake Spectra* 30 (3): 973–987. <https://doi.org/10.1193/072113EQS209M>.
- Bradley, B. A. 2010. "A Generalized Conditional Intensity Measure Approach and Holistic Ground-Motion Selection." *Earthquake Engineering & Structural Dynamics* 39 (12): 1321–1342. <https://doi.org/10.1002/eqe.995>.
- Bradley, B. A. 2012. "The Seismic Demand Hazard and Importance of the Conditioning Intensity Measure." *Earthquake Engineering & Structural Dynamics* 41 (11): 1417–1437. <https://doi.org/10.1002/eqe.2221>.
- Bradley, B. A., R. P. Dhakal, G. A. MacRae, and M. Cubrinovski. 2009. "Prediction of Spatially Distributed Seismic Demands in Specific Structures: Ground Motion and Structural Response." *Earthquake Engineering & Structural Dynamics* 39 (5): 501–520. <https://doi.org/10.1002/eqe.954>.
- Caltrans. 2010. *Caltrans Seismic Design Criteria Version 1.6*. California Department of Transportation. Sacramento, CA: State of California. <https://dot.ca.gov/programs/engineering-services/manuals/seismic-design-criteria>
- Caltrans. 2019. *Caltrans Seismic Design Criteria Version 2.0*. California Department of Transportation. Sacramento, CA: State of California. <https://dot.ca.gov/programs/engineering-services/manuals/seismic-design-criteria>
- Campbell, K. W., and Y. Bozorgnia. 2008. "NGA Ground Motion Model for the Geometric Mean Horizontal Component of PGA, PGV, PGD and 5% Damped Linear Elastic Response Spectra for Periods Ranging from 0.01 to 10 S." *Earthquake Spectra* 24 (1): 139–171. <https://doi.org/10.1193/1.2857546>.
- Chandramohan, R., J. W. Baker, and G. G. Deierlein. 2016. "Quantifying the Influence of Ground Motion Duration on Structural Collapse Capacity Using Spectrally Equivalent Records." *Earthquake Spectra* 32 (2): 927–950. <https://doi.org/10.1193/122813EQS298MR2>.
- Cordova, P. P., G. G. Deierlein, S. S. F. Mehanny, and C. A. Cornell. 2000. "Development of a Two-Parameter Seismic Intensity Measure and Probabilistic Assessment Procedure." In *Second US-Japan Working Performance-Based Earthquake Engineering Methodology Reinforced Concrete Building Structure*, edited by T. Kabeyasawa, and J. P. Moehle, 187–206. Hokkaido: Journal of Engineering and Applied Science.
- Cornell, C. A., and H. Krawinkler. 2000. "Progress and Challenges in Seismic Performance Assessment." *PEER Center News* 3 (2): 1–2.
- Dávalos, H., P. Heresi, and E. Miranda. 2020. "A Ground Motion Prediction Equation for Filtered Incremental Velocity, FIV3." *Soil Dynamics and Earthquake Engineering* 139:106346. <https://doi.org/10.1016/j.soildyn.2020.106346>.
- Dávalos, H., and E. Miranda. 2019. "Filtered Incremental Velocity: A Novel Approach in Intensity Measures for Seismic Collapse Estimation." *Earthquake Engineering & Structural Dynamics* 48 (12): 1384–1405. <https://doi.org/10.1002/eqe.3205>.
- Dávalos, H., and E. Miranda. 2021. "A Ground Motion Prediction Model for Average Spectral Acceleration." *Journal of Earthquake Engineering* 25 (2): 319–342. <https://doi.org/10.1080/13632469.2018.1518278>.
- Duncan, J. M., and R. L. Mokwa. 2001. "Passive Earth Pressures: Theories and Tests." *Journal of Geotechnical and Geoenvironmental Engineering* 127 (3): 248–257. [https://doi.org/10.1061/\(ASCE\)1090-0241\(2001\)127:3\(248\)](https://doi.org/10.1061/(ASCE)1090-0241(2001)127:3(248)).
- Eads, L., and E. Miranda. 2013. *Seismic collapse risk assessment of buildings: effects of intensity measure selection and computational approach*. Report No. 184. Stanford, California: Stanford University.
- Enke, D. L., C. Tirarachai, and R. Luna. 2008. "Estimation of Earthquake Loss Due to Bridge Damage in the St. Louis Metropolitan Area. II: Indirect Losses." *Natural Hazards Review* 9 (1): 12–19. [https://doi.org/10.1061/\(ASCE\)1527-6988\(2008\)9:1\(12\).](https://doi.org/10.1061/(ASCE)1527-6988(2008)9:1(12).)
- Fayaz, J., M. Dabaghi, and F. Zareian. 2020a. "Utilization of Site-Based Simulated Ground Motions for Hazard-Targeted Seismic Demand Estimation: Application for Ordinary Bridges in Southern California." *Journal of Bridge Engineering* 25 (11). [https://doi.org/10.1061/\(ASCE\)BE.1943-5592.0001634](https://doi.org/10.1061/(ASCE)BE.1943-5592.0001634).
- Fayaz, J., M. Medalla, and F. Zareian. 2020b. "Sensitivity of the Response of Box-Girder Seat-Type Bridges to the Duration of Ground Motions Arising from Crustal and Subduction Earthquakes." *Engineering Structures* 219:110845. <https://doi.org/10.1016/j.engstruct.2020.110845>.
- Feng, R., X. Wang, W. Yuan, and J. Yu. 2018. "Impact of Seismic Excitation Direction on the Fragility Analysis of Horizontally Curved Concrete Bridges." *Bulletin of Earthquake Engineering* 16 (10): 4705–4733. <https://doi.org/10.1007/s10518-018-0400-2>.
- Feng, R., W. Yuan, and A. Sextos. 2021. "Probabilistic Loss Assessment of Curved Bridges Considering the Effect of Ground Motion Directionality." *Earthquake Engineering & Structural Dynamics* 50 (13): 3623–3645. <https://doi.org/10.1002/eqe.3525>.
- Gardoni, P., A. Der Kiureghian, and K. M. Mosalam. 2002. "Probabilistic Capacity Models and Fragility Estimates for Reinforced Concrete Columns Based on Experimental Observations." *Journal of Engineering Mechanics* 128 (10): 1024–1038. [https://doi.org/10.1061/\(ASCE\)0733-9399\(2002\)128:10\(1024\).](https://doi.org/10.1061/(ASCE)0733-9399(2002)128:10(1024).)



- Giannopoulos, D., and D. Vamvatsikos. 2018. "Ground Motion Records for Seismic Performance Assessment: To Rotate or Not to Rotate?" *Earthquake Engineering & Structural Dynamics* 47 (12): 2410–2425. <https://doi.org/10.1002/eqe.3090>.
- Haselton, C. B., and J. W. Baker. 2006. "Ground Motion Intensity Measures for Collapse Capacity Prediction: Choice of Optimal Spectral Period and Effect of Spectral Shape." *8th US National Conference on Earthquake Engineering* 15:8830–8839. <https://api.semanticscholar.org/CorpusID:124847110>.
- HAZUS. 2003. *Multi-Hazard Loss Estimation Methodology - Earthquake Model*. Washington, DC, USA: FEMA-National Institute of Building Sciences.
- Heresi, P., H. Dávalos, and E. Miranda. 2018. "Ground Motion Prediction Model for the Peak Inelastic Displacement of Single-Degree-Of-Freedom Bilinear Systems." *Earthquake Spectra* 34 (3): 1177–1199. <https://doi.org/10.1193/061517EQS118M>.
- Huang, Q., P. Gardoni, and S. Hurlebaus. 2010. "Probabilistic Seismic Demand Models and Fragility Estimates for Reinforced Concrete Highway Bridges with One Single-Column Bent." *Journal of Engineering Mechanics* 136 (11): 1340–1353. [https://doi.org/10.1061/\(ASCE\)EM.1943-7889.0000186](https://doi.org/10.1061/(ASCE)EM.1943-7889.0000186).
- Kalkan, E., and S. K. Kunath. 2006. "Effects of Fling Step and Forward Directivity on Seismic Response of Buildings." *Earthquake Spectra* 22 (2): 367–390. <https://doi.org/10.1193/1.2192560>.
- Kaviani, P., F. Zareian, and E. Taciroglu. January 2014. "Performance-Based Seismic Assessment of Skewed Bridges." *Pacific Earthquake Engineering Research Center* 161. <https://doi.org/10.13140/2.1.1586.0007>.
- Kazantzi, A. K., and D. Vamvatsikos. 2015. "Intensity Measure Selection for Vulnerability Studies of Building Classes." *Earthquake Engineering & Structural Dynamics* 44 (15): 2677–2694. <https://doi.org/10.1002/eqe.2603>.
- Kilanitis, I., and A. Sextos. 2019. "Impact of Earthquake-Induced Bridge Damage and Time Evolving Traffic Demand on the Road Network Resilience." *Journal of Traffic and Transportation Engineering (English Edition)* 6 (1): 35–48. <https://doi.org/10.1016/j.jtte.2018.07.002>.
- Kohrangi, M., P. Bazzurro, D. Vamvatsikos, and A. Spillatura. 2017. "Conditional Spectrum-Based Ground Motion Record Selection Using Average Spectral Acceleration." *Earthquake Engineering & Structural Dynamics* 46 (10): 1667–1685. <https://doi.org/10.1002/eqe.2876>.
- Kohrangi, M., S. R. Kotha, and P. Bazzurro. 2018. "Ground-Motion Models for Average Spectral Acceleration in a Period Range: Direct and Indirect Methods." *Bulletin of Earthquake Engineering* 16 (1): 45–65. <https://doi.org/10.1007/s10518-017-0216-5>.
- Lin, T., C. B. Haselton, and J. W. Baker. 2013. "Conditional Spectrum-Based Ground Motion Selection. Part II: Intensity-Based Assessments and Evaluation of Alternative Target Spectra." *Earthquake Engineering & Structural Dynamics* 42 (12): 1867–1884. <https://doi.org/10.1002/eqe.2303>.
- Lin, Y., X. He, and A. Igarashi. 2022. "Influence of Directionality of Spectral-Compatible Bi-Directional Ground Motions on Critical Seismic Performance Assessment of Base-Isolation Structures." *Earthquake Engineering & Structural Dynamics* 51 (6): 1477–1500. <https://doi.org/10.1002/eqe.3624>.
- Luco, N., and C. A. Cornell. 2007. "Structure-Specific Scalar Intensity Measures for Near-Source and Ordinary Earthquake Ground Motions." *Earthquake Spectra* 23 (2): 357–392. <https://doi.org/10.1193/1.2723158>.
- Mackie, K. R., K. J. Cronin, and B. G. Nielson. 2011. "Response Sensitivity of Highway Bridges to Randomly Oriented Multi-Component Earthquake Excitation." *Journal of Earthquake Engineering* 15 (6): 850–876. <https://doi.org/10.1080/13632469.2010.551706>.
- Mangalathu, S., J.-S. Jeon, J. E. Padgett, and R. DesRoches. 2017. "Performance-Based Grouping Methods of Bridge Classes for Regional Seismic Risk Assessment: Application of ANOVA, ANCOVA, and Non-Parametric Approaches." *Earthquake Engineering & Structural Dynamics* 46 (14): 2587–2602. <https://doi.org/10.1002/eqe.2919>.
- Mehdizadeh, M., K. R. Mackie, and B. G. Nielson. 2017. "Scaling Bias and Record Selection for Quantifying Seismic Structural Demand." *Journal of Structural Engineering* 143 (9): 1–12. [https://doi.org/10.1061/\(asce\)st.1943-541x.0001855](https://doi.org/10.1061/(asce)st.1943-541x.0001855).
- Monteiro, R., C. Zelaschi, A. Silva, and R. Pinho. 2019. "Derivation of Fragility Functions for Seismic Assessment of RC Bridge Portfolios Using Different Intensity Measures." *Journal of Earthquake Engineering* 23 (10): 1678–1694. Taylor & Francis. <https://doi.org/10.1080/13632469.2017.1387188>.
- O'Reilly, G. J. 2021. "Limitations of Sa(t) As an Intensity Measure When Assessing Non-Ductile Infilled RC Frame Structures." *Bulletin of Earthquake Engineering* 19 (6): 2389–2417. <https://doi.org/10.1007/s10518-021-01071-7>.
- Omrani, R., B. Mobasher, S. Sheikhakbari, F. Zareian, and E. Taciroglu. 2017. "Variability in the Predicted Seismic Performance of a Typical Seat-Type California Bridge Due to Epistemic Uncertainties in Its Abutment Backfill and Shear-Key Models." *Engineering Structures* 148: 718–738. <https://doi.org/10.1016/j.engstruct.2017.07.018>.
- Otárola, K., J. Fayaz, and C. Galasso. 2022. "Fragility and Vulnerability Analysis of Deteriorating Ordinary Bridges Using Simulated Ground-Motion Sequences." *Earthquake Engineering & Structural Dynamics* 51 (13): 3215–3240. <https://doi.org/10.1002/eqe.3720>.
- Petrini, L., C. Maggi, M. J. N. Priestley, and G. M. Calvi. 2008. "Experimental Verification of Viscous Damping Modeling for Inelastic Time History Analyzes." *Journal of Earthquake Engineering* 12 (SUPPL. 1): 125–145. <https://doi.org/10.1080/13632460801925822>.

- Poulos, A., and E. Miranda. 2023. "Modification of Ground-Motion Models to Estimate Orientation-Dependent Horizontal Response Spectra in Strike-Slip Earthquakes." *Bulletin of the Seismological Society of America* 113 (6): 2718–2729. <https://doi.org/10.1785/0120230084>.
- Priestley, M. J. N., F. Seible, and G. M. Calvi. 1996. *Seismic Design and Retrofit of Bridges*. New York: John Wiley & Sons.
- Qian, J., and Y. Dong. 2020. "Multi-Criteria Decision Making for Seismic Intensity Measure Selection Considering Uncertainty." *Earthquake Engineering & Structural Dynamics* 49 (11): 1095–1114. <https://doi.org/10.1002/eqe.3280>.
- Rivera-Figueroa, A., and L. A. Montejo. 2022. "Spectral Matching RotD100 Target Spectra: Effect on Records Characteristics and Seismic Response." *Earthquake Spectra* 38 (2): 1570–1586. <https://doi.org/10.1177/87552930211049259>.
- Romstad, K. M., B. Kutter, B. Maroney, E. Varderbilt, M. Griggs, and Y. H. Chai. 1995. *Experimental Measurements of Bridge Abutment Behavior. Report No. UCD STR 95 1*. Davis, CA: University of California, Structural Engineering Group.
- Scott, M. H., and G. L. Fenves. 2006. "Plastic Hinge Integration Methods for Force-Based Beam-Column Elements." *Journal of Structural Engineering* 132 (2): 244–252. [https://doi.org/10.1061/\(asce\)0733-9445\(2006\)132:2\(244\)](https://doi.org/10.1061/(asce)0733-9445(2006)132:2(244)).
- Scott, M. H., and K. L. Ryan. 2013. "Moment-Rotation Behavior of Force-Based Plastic Hinge Elements." *Earthquake Spectra* 29 (2): 597–607. <https://doi.org/10.1193/1.4000136>.
- Sengupta, A., L. Quadery, S. Sarkar, and R. Roy. 2016. "Influence of Bidirectional Near-Fault Excitations on RC Bridge Piers." *Journal of Bridge Engineering* 21 (7). [https://doi.org/10.1061/\(asce\)be.1943-5592.0000836](https://doi.org/10.1061/(asce)be.1943-5592.0000836).
- Shahri, S. K., and J. W. Baker. 2014. "NGA-West2 Models for Ground Motion Directionality." *Earthquake Spectra* 30 (3): 1285–1300. <https://doi.org/10.1193/040913EQS097M>.
- Shamsabadi, A., K. M. Rollins, and M. Kapuskar. 2007. "Nonlinear Soil–Abutment–Bridge Structure Interaction for Seismic Performance-Based Design." *Journal of Geotechnical and Geoenvironmental Engineering* 133 (6): 707–720. [https://doi.org/10.1061/\(asce\)1090-0241\(2007\)133:6\(707\)](https://doi.org/10.1061/(asce)1090-0241(2007)133:6(707)).
- Shome, N., C. A. Cornell, P. Bazzurro, and J. E. Carballo. 1998. "Earthquakes, Records, and Nonlinear Responses." *Earthquake Spectra* 14 (3): 469–500. <https://doi.org/10.1193/1.1586011>.
- Somerville, P. G., N. F. Smith, R. W. Graves, and N. A. Abrahamson. 1997. "Modification of Empirical Strong Ground Motion Attenuation Relations to Include the Amplitude and Duration Effects of Rupture Directivity." *Seismological Research Letters* 68 (1): 199–222. <https://doi.org/10.1785/gssrl.68.1.199>.
- Sousa, L., V. Silva, M. Marques, and H. Crowley. 2016. "On the Treatment of Uncertainties in the Development of Fragility Functions for Earthquake Loss Estimation of Building Portfolios." *Earthquake Engineering & Structural Dynamics* 45 (12): 1955–1976. <https://doi.org/10.1002/eqe.2734>.
- Sousa, R., J. P. Almeida, A. A. Correia, and R. Pinho. 2020. "Shake Table Blind Prediction Tests: Contributions for Improved Fiber-Based Frame Modelling." *Journal of Earthquake Engineering* 24 (9): 1435–1476. <https://doi.org/10.1080/13632469.2018.1466743>.
- Stewart, J., E. Taciroglu, J. Wallace, E. Ahlberg, A. Lemnitzer, C. Rha, P. Tehrani, S. Keowen, R. Nigbor, and A. Salamanca. 2007. *Full Scale Cyclic Testing of Foundation Support Systems for Highway Bridges. Part II: Abutment Backwalls. Report No. UCLA SGEL 2007/02*. Los Angeles, CA: University of California.
- Tarbali, K. 2017. "Ground Motion Selection for Seismic Response Analysis." PhD diss., Christchurch, New Zealand: University of Canterbury.
- Torbol, M., and M. Shinozuka. 2014. "The Directionality Effect in the Seismic Risk Assessment of Highway Networks." *Structure and Infrastructure Engineering* 10 (2): 175–188. <https://doi.org/10.1080/15732479.2012.716069>.
- Tothong, P., and C. A. Cornell. 2006. "An Empirical Ground-Motion Attenuation Relation for Inelastic Spectral Displacement." *Bulletin of the Seismological Society of America* 96 (6): 2146–2164. <https://doi.org/10.1785/0120060018>.
- Tothong, P., and N. Luco. 2007. "Probabilistic Seismic Demand Analysis Using Advanced Ground Motion Intensity Measures." *Earthquake Engineering & Structural Dynamics* 36 (13): 1837–1860. <https://doi.org/10.1002/eqe.696>.
- Vamvatsikos, D., and C. A. Cornell. 2002. "Incremental Dynamic Analysis." *Earthquake Engineering & Structural Dynamics* 31 (3): 491–514. <https://doi.org/10.1002/eqe.141>.
- Vamvatsikos, D., and C. A. Cornell. 2005. "Developing Efficient Scalar and Vector Intensity Measures for IDA Capacity Estimation by Incorporating Elastic Spectral Shape Information." *Earthquake Engineering & Structural Dynamics* 34 (13): 1573–1600. <https://doi.org/10.1002/eqe.496>.
- Wilson, P., and A. Elgamal. 2006. "Large Scale Measurement of Lateral Earth Pressure on Bridge Abutment Back-Wall Subjected to Static and Dynamic Loading." In *Proceedings of the New Zealand workshop on Geotechnical Earthquake Engineering*, edited by M. Cubrinovski, 307–315. Christchurch, New Zealand: University of Canterbury.
- Wu, Y. F., A. Q. Li, and H. Wang. 2019. "Inelastic Displacement Spectra for Chinese Highway Bridges Characterized by Single-Degree-Of-Freedom Bilinear Systems." *Advances in Structural Engineering* 22 (14): 3066–3085. <https://doi.org/10.1177/1369433219857845>.
- Zhu, M., F. McKenna, and M. H. Scott. 2018. "OpenSeespy: Python Library for the OpenSees Finite Element Framework." *SoftwareX* 7: 6–11. <https://doi.org/10.1016/j.softx.2017.10.009>.